Author Manuscript

Author Manuscript

Author Manuscript

Author Manuscript

HHS Public Access

Author manuscript

J Bone Miner Res. Author manuscript; available in PMC 2018 June 01.

Published in final edited form as:

J Bone Miner Res. 2017 June ; 32(6): 1354–1367. doi:10.1002/jbmr.3108.

Fkbp10 Deletion in Osteoblasts leads to Qualitative Defects in Bone

Caressa D. Lietman[1], **Joohyun Lim**[1], **Ingo Grafe**[1], **Yuqing Chen**[1], **Hao Ding**[2], **Xiaohong Bi**[2], **Catherine G. Ambrose**[3], **Nadja Fratzl-Zelman**[4], **Paul Roschger**[4], **Klaus Klaushofer**[4], **Wolfgang Wagermaier**[5], **Ingo Schmidt**[5], **Peter Fratzl**[5], **Jyoti Rai**[6], **MaryAnn Weis**[6], **David Eyre**[6], **Douglas R. Keene**[7], **Deborah Krakow**[8], and **Brendan H. Lee**[1]

[1]Department of Molecular and Human Genetics, Baylor College of Medicine, Houston, TX 77030, USA

[2]Department of Nanomedicine and Biomedical Engineering, University of Texas Health Science Center at Houston, Houston, TX 77054, USA

[3]Department of Orthopaedic Surgery, University of Texas Health Science Center at Houston, Houston, TX 77030, USA

[4]Ludwig Boltzmann Institute of Osteology, Hanusch Hospital of WGKK and AUVA Trauma Centre Meidling 1st Med. Dept. Hanusch Hospital, Heinrich Collin Str. 30, 1140, Vienna, Austria

[5]Department of Biomaterials, Max Planck Institute of Colloids and Interfaces, Research Campus Golm, Potsdam 14424, Germany

[6]Department of Orthopaedics and Sports Medicine, University of Washington, Seattle, WA 98195, USA

[7]Micro-Imaging Center, Shriners Hospital for Children, Portland, OR 97239, USA

[8]Department of Orthopaedic Surgery, David Geffen School of Medicine at UCLA, Los Angeles, CA 90095, USA

Abstract

Osteogenesis Imperfecta (OI), also known as brittle bone disease, displays a spectrum of clinical severity from mild (OI type I) to severe early lethality (OI type II), with clinical features including low bone mass, fractures and deformities. Mutations in the FK506 Binding Protein 10 (*FKBP10*), gene encoding the 65KDa protein FKBP65, cause a recessive form of OI and Bruck syndrome, the latter being characterized by joint contractures in addition to low bone mass. We previously showed that *Fkbp10* expression is limited to bone, tendon and ligaments in postnatal tissues. Furthermore, in both patients and *Fkbp10* knockout mice, collagen telopeptide hydroxylysine

Corresponding Author: Brendan Lee, M.D., Ph.D., Department of Molecular and Human Genetics, Baylor College of Medicine, One Baylor Plaza, Room R814, Houston, TX 77030, Fax number: 713-798-5168, Telephone number: 713-798-8853, blee@bcm.edu.

Supplemental information is included with this manuscript.

Authors' roles: Study design: CL. Study conduct: CL, IG, JL, YC, HD, XB, CA, NFZ, PR, KK, WW, IS, PF, JR, MW, DK. Data collection: CL, JL, IG, NFZ, PR, CA, XB, PF, MW. Data analysis: CL, IG, CA, XB, PR, NFZ, PF, MW, DE. Data interpretation: all authors. Drafting manuscript: CL and BL. Revising manuscript content: all authors. Approving final version of manuscript: all authors. BL takes responsibility for the integrity of the data analysis.

Author Manuscript Author Manuscript Author Manuscript Author Manuscript

crosslinking is dramatically reduced. To further characterize the bone specific contributions of *Fkbp10*, we conditionally ablated FKBP65 in *Fkbp10*$^{fl/fl}$ mice (*Mus musculus*; C57BL/6) using the osteoblast specific *Col1a1* 2.3kb Cre recombinase. Using μCT, histomorphometry and quantitative backscattered electron imaging, we found minimal alterations in the quantity of bone and no differences in the degree of bone matrix mineralization in this model. However, mass spectroscopy of bone collagen demonstrated a decrease in mature, hydroxylysine-aldehyde crosslinking. Furthermore, bone of mutant mice exhibits a reduction in mineral-to-matrix ratio and in crystal size as shown by Raman spectroscopy and small angle x-ray scattering, respectively. Importantly, abnormalities in bone quality were associated with impaired bone biomechanical strength in mutant femurs compared with those of wild type littermates. Taken together, these data suggest that the altered collagen crosslinking through *Fkbp10* ablation in osteoblasts primarily leads to a qualitative defect in the skeleton.

Keywords

osteogenesis imperfecta; matrix mineralization; collagen; osteoblasts; genetic animal models

Introduction

Bone is comprised of two integral components, collagen fibers (primarily type I collagen) and mineral nanocrystals of hydroxyapatite (1, 2). Type I collagen is synthesized in the endoplasmic reticulum (ER) as two α1 chains, and one α2 chain that acquire many posttranslational modifications before assembly into the triple-helical procollagen molecules that polymerize into fibrils of the extracellular matrix. After secretion, propeptides at the C and N terminus are cleaved, and the processed molecules become cross-linked by lysyl oxidase (*LOX*) as mature fibrils grow. The crosslinks are essential for normal fibril stability, mineralization and material properties of bone (1). In the type I collagen molecule, there are two helical and two telopeptide lysine locations where enzymatic crosslinking can occur. The resulting cross-linking chemistry is modulated in a tissue-specific manner by the degree of hydroxylation of these lysines that is controlled by the lysyl hydroxylases (LH1 and LH2, encoded by *PLOD1* and *PLOD2*, respectively) (1). In previous studies, decreased cross-linking by inhibition of lysyl oxidase (*LOX*) was shown to reduce bone strength (1, 3–5). Furthermore, it has been proposed that fewer crosslinks could be a determinant of impaired bone mechanical properties in aging, osteoporosis and diabetes mellitus due to their effect on the mineralization process (6).

The degree of mineralization, and the quality of the mineral (i.e. number, size, perfection and organization of the crystals relative to the cross-linked collagen polymers) plays a role in the biomechanical properties of bone (7). The mineral nanocrystal organization is dependent upon the organic matrix, mainly comprised of collagen, and its structural arrangement (7). Thus, the biomechanical strength of bone to resist fractures is dependent on the quantity of bone as well as the quality, for instance microarchitecture and matrix composition (8).

Mutations in the type I collagen genes (*COL1A1* and *COL1A2*) lead to qualitative and quantitative defects in collagen production, and account for the majority of cases of

Author Manuscript Author Manuscript Author Manuscript Author Manuscript

Osteogenesis Imperfecta (OI) (9). OI, also known as brittle bone disease, is a connective tissue disorder which is characterized by bone fragility and low bone mass, with varying severity (9). Importantly, mutations in several additional genes can cause OI, most of which are involved with defective posttranslational modifications of type I collagen. While mutations in *CRTAP* (HGNC: 2379), *LEPRE1* and *PPIB* result in defective prolyl-3-hydroxylation, mutations in *FKBP10* and *PLOD2* lead to defective lysine hydroxylation at the telopeptide crosslinking sites (2, 10–15).

FKBP10 encodes FKBP65, a chaperone molecule with prolyl cis-trans isomerase activity (PPIase) that appears to interact with collagen and elastin in the endoplasmic reticulum (16–21). Patients with homozygous mutations resulting in the lack of FKBP65 protein exhibit a phenotypic spectrum of OI, Bruck syndrome (characterized by OI and additional joint contractures, that can also be caused by mutations in *PLOD2*), and Kuskokwim syndrome (a rare recessive disorder with joint contractures, but a mild bone phenotype) (11, 13, 22, 23). Interestingly, bone collagen of patients with *FKBP10* mutations shows a lack of telopeptide lysine hydroxylation and resulting abnormal collagen crosslinking, similar to that observed in patients with mutations in *PLOD2* (LH2) (23). Recently, we have shown a reduction in telopeptide lysine hydroxylation in a mouse model with systemic deletion of *Fkbp10* (24). These knockout mice demonstrated generalized connective tissue defects, but also exhibited perinatal lethality, and thus the bone specific role of *Fkbp10* could not be fully evaluated (24).

In this study, we utilized mice with a conditional *Fkbp10* allele in combination with the osteoblast specific *Col1a1* Cre recombinase allele to examine the bone specific effects of *Fkbp10* ablation and the implications of defective collagen telopeptide crosslinking in bone. This study tests the hypothesis that defective collagen telopeptide crosslinking in bone would lead to changes in the quality of bone including biomechanical strength, composition, and crystalline structure, which may contribute to the bone phenotypes leading to both OI and Bruck syndrome. Hence, this study not only explores the role of *Fkbp10* in OI, but also in the larger context of abnormal collagen crosslinking, with potential implications in other forms of skeletal fragility.

Materials and Methods

Animal housing and genotyping

ES cells (clone EPD0142_1_A09, parental strain JM8A3.N1) were obtained from EUCOMM (25) and injected in-house (Baylor College of Medicine). Mice were maintained on a C57BL/6J background. Mice were housed in the Baylor College of Medicine vivarium with 2–5 mice per cage and were fed *ad libitum* with standard mouse diet (Land O'Lakes Purina Animal Nutrition, 5V5R 3002906-703). The facility is specific pathogen free for the following agents: mouse adenovirus (MAV 1&2), mouse cytomegalovirus, ectromelia, murine minute virus, mouse parvovirus, Polyomavirus, mouse hepatitis virus, Hantaviruses, lymphocytic choriomeningitis virus, pneumonia virus of mice, reovirus 3, mouse rotavirus, Sendai virus, Theiler's mouse encephalomyelitis virus, *Mycoplasma pulmonis*, endoparasites and ectoparasites.

Author Manuscript Author Manuscript Author Manuscript Author Manuscript

These studies were approved by the Baylor College of Medicine Institutional Animal Care and Use Committee as well as Center for Comparative Medicine (protocol number AN-1506). Euthanasia was performed using approved methods via carbon dioxide gas. Genotyping was performed using primers flanking exon 2 for the wild type allele (5′AATAGGTAGCACACAGTTCGG3′) and (5′GTGAACAGTATGACCTTGGCC3′). The mutant allele was identified by primers in the Bactin:neo cassette (5′AGCGTGCGCCGTTCCGAAAGT3′) and (5′GGCGGCGGTGGAATCGAAATC3′) as well as primers specific for the last loxP site (5′GGAGCGAAGGAGGATTACTGTGCC3′) and (5′TGAACTGATGGCGAGCTCAGACC3′). Animals were allocated into two groups for all studies: littermates that were homozygous floxed (fl/fl) with or without the Col1a1 Cre. The same mice were utilized for μCT, Raman spectroscopy, 3pt bending, mass spectrometry, and histomorphometric analysis. A separate group was used for quantitative backscattered electron imaging (qBEI) and small-angle X ray scattering (SAXS) measurements. A third group was collected for electron microscopy studies. Male mice were used for all studies; males and females were utilized for μCT, qBEI and SAXS analysis. All mice were 3 months old at the time of tissue collection. A single mouse was used for the following: right femur fixed in formalin for μCT analysis followed by plastic embedding and histomorphometry; left femur wrapped in sterile gauze soaked in saline and stored at −20°C for 3-point bending analysis; left tibia stored in 70% EtOH for Raman spectroscopy; calvaria collected and immediately snap-frozen in liquid nitrogen for western blotting. A separate mouse was used for the following: left femur stored in 70% EtOH for qBEI followed by SAXS of the same femur; right femur and tibia collected and immediately snap-frozen in liquid nitrogen for mass spectrometry analysis. A third group was used for the femurs for electron microscopy. All samples were consistently collected from the same location.

Animals used per experiment as follows: μCT (9 male control, 7 male experimental, 10 female controls and experimental); 3pt bending (6 and 8 males); Raman (7 males per group); MS (3 male per group in figure it says 3–4); SAXS (3 male controls and mutants, 4 female controls and mutants); qBEI (3 male control and experimental, 4 female controls and experimental); EM (3 males per group); Western (2 representative samples shown, both males and females were tested with 3 per group). N is indicated throughout manuscript.

Western blotting

Calvaria and long bones were collected from control and mutant mice at 3 months of age. Calvaria were cut into strips and long bones were removed of the epiphyses and bone marrow and frozen in liquid nitrogen. Samples were then homogenized in SDS protein buffer, boiled, then concentrated. They were then loaded onto 4–15% gradient SDS-PAGE gels (Bio-Rad). Protein was transferred to PVDF membrane and blocked with 5% nonfat dry milk/ PBS. Blots were probed with either polyclonal rabbit anti-FKBP65 antibody (Proteintech Group) at 1:5000 and co-incubated with monoclonal mouse-anti tubulin at 1:10000 in 1% milk overnight at 4°C. Blots were washed with PBST. Secondary antibodies (anti-rabbit 488 and anti-mouse 594 Odyssey LiCor) were diluted 1:10,000 in 1% milk plus PBST for 1 hour at room temperature. The Odyssey system was used to image the blots by fluorescence (LiCor).

Author Manuscript Author Manuscript Author Manuscript Author Manuscript

Skeletal analyses and bone histomorphometry

Radiographs of mutant mice and their respective littermates were taken (identical views) with the Kubtec XPERT80 (Kubtec X-ray, Milford, CT). To analyze bone phenotypes, femurs and vertebrae were isolated at 3 months of age. The bones were fixed in 10% buffered formalin for 48h for subsequent analysis. Radiography of bones was performed with an Xpert 80 system (Kubtec). Spines and right femurs were scanned in 70% ethanol using a Scanco μCT-40 microCT system (55kVp and 145μA X-ray source) and scans were reconstructed at a 16μm isotropic voxel size. Trabecular bone of L4 vertebrae and the distal metaphyseal part of right femurs were analyzed using Scanco software by manually contouring trabecular bone. For vertebrae, the region of interest (ROI) was defined as the trabecular volume between the L4 vertebral endplates. As femoral trabecular ROI 75 slices (=1.2 mm) were analyzed proximal to the distal femoral growth plate. Quantification of trabecular parameters was performed using the Scanco software with a threshold value of 210. These parameters include bone volume/total volume (BV/TV), trabecular number (Tb.N), trabecular thickness (Tb.Th), trabecular separation (Tb.Sp) and tissue mineral density (TMD). Femur length was measured from the top of the femoral head to the bottom of the medial condyle. Cortical bone parameters of the femoral midshaft including cortical thickness (Ct.Th) and tissue mineral density (TMD) were measured using 50 slices immediately below the trochanter. Standard methods and abbreviations are used (26).

Calcein was injected 7 and 2 days before sacrifice and lumbar vertebrae (L4) were used to generate plastic sections to assess dynamic histomorphometry. Specifically, lumbar vertebrae were embedded in methyl methacrylate, and embedded samples were sectioned using tungsten carbide blades. Images of a complete plane of section from L4 from each mouse were acquired and used for evaluation of bone formation parameters including the mineral apposition rate (MAR) and bone formation rate (BFR/BS). Von Kossa staining was used to calculate bone volume and osteoid parameters (OV/BV and OS/BS). Tartrate-resistant acid phosphatase staining was used to quantify osteoclast numbers (N.Oc/BS) and surfaces (Oc.S/BS), and trichrome staining was used to quantify osteoblast numbers (N.Ob/BS), surface (Ob.S/BS) and osteocyte density (N.Ot/B.Ar.). All histomorphometric analyses were performed with Bioquant Osteo software (Bioquant). Standard nomenclature was used (27).

Collagen cross-link and mass spectral analyses

Pyridinoline cross-links (HP and LP) were quantified by HPLC after hydrolyzing saline washed bone in 6N HCl as described (28). Briefly, samples were dried and redissolved in 1% (v/v) n-heptafluorobutyric acid and run on an Agilent 1260 HPLC (Agilent Technologies) using a C18 RP-HPLC (Brownlee Aquapore RP-300 7u, 250x4.6mm, Perkin Elmer) running at 1 ml/min. Samples were eluted with a linear gradient of 17–21% acetonitrile in a running buffer of 0.01 M n-heptafluorobutyric acid in water. Type I collagen was prepared from bone decalcified at 4°C in 0.1M HCl overnight. Demineralized bone was treated with CNBr in 70% formic acid at room temperature for 24hrs and freeze-dried. CNBr peptides were run on 12.5% SDS-PAGE using the method of Laemmli. Femurs and tibias were both used and analyzed separately. CB peptide bands were cut from SDS-PAGE gels and digested with trypsin in-gel (29). Peptides were analyzed by electrospray LC/MS using an LTQ XL ion-trap mass spectrometer (Thermo Scientific) equipped with in-line

Author Manuscript Author Manuscript Author Manuscript Author Manuscript

liquid chromatography using a C4 5um capillary column (300 um×150 mm; Higgins Analytical RS-15M3-W045) eluted at 4.5 μl min. The LC mobile phase consisted of buffer A (0.1% formic acid in MilliQ water) and buffer B (0.1% formic acid in 3:1 acetonitrile:n-propanol v/v). An electrospray ionization source (ESI) introduced the LC sample stream into the mass spectrometer with a spray voltage of 4 kV. Proteome Discoverer search software (Thermo Scientific) was used for peptide identification using the NCBI protein database. Large collagenous peptides not found by Sequest had to be identified manually by calculating the possible ms/ms ions and matching these to the actual ms/ms. Hydroxyproline and hydroxylysine calculations were done manually by scrolling or averaging the full scan over several minutes so that all of the post-translational variations of a given peptide appeared together in the full scan.

Biomechanical Testing

Femurs were tested in three-point bending using a span of 6.21mm using an Instron 5848 device (Instron Inc., Norwood MA). Prior to mechanical testing, bones were thawed, soaked in saline for at least 30 minutes, and then tested wet at room temperature. They were preloaded in the anterior to posterior direction (anterior side in compression, posterior side in tension) to 1N for 5 seconds and then were compressed to failure at a rate of 0.1mm/sec. Load and displacement data was captured at rate of 40Hz by using BLUEHILL Software (Instron). Following testing, all data files were analyzed using a MatLab program written to extract the pertinent data. Stress was calculated using the following formula:

$$Stress = \frac{(0.5h)\,FL}{4I}$$

where F is the load applied on the femur in N, L is the span length in mm, h is the specimen diameter in mm, and I is the cross-sectional moment of inertia in mm^4. Both h and I were obtained by analyzing a midshaft micro-CT image from femurs stored in saline soaked gauze (separate from the full μCT analysis). Strain was calculated using the following formula:

$$Strain = \frac{6Dh}{L^2}$$

where D is the actuator displacement in mm, h is the diameter in mm and L is the span length in mm. The load-displacement curve was divided into 4 equal segments from the end of the preload to the maximum load, and the slope of each segment was calculated. Stiffness and Elastic Modulus were defined from this maximum slope of the load-displacement and the corresponding slope of the stress-strain curve, respectively. Yield points were determined on both the load-displacement and stress-strain curves using a 0.2% offset strain from the maximum slope of the linear portion of the curve. The elastic region was identified as the region from the completion of the preload to the Yield Point. The plastic region was identified as the region from the Yield Point until the Failure Point. Failure was defined as fracture. A trapezoidal numerical integration method was used to determine both energy (area under the load-displacement curve) and resilience (area under elastic portion of the

Author Manuscript Author Manuscript Author Manuscript Author Manuscript

stress-strain curve). Maximum Load and ultimate strength were determined by finding the highest load and strength values recorded by BLUEHILL, before the specimen failed.

Raman spectroscopy

Raman spectra were acquired from the cortex of intact tibiae using a confocal Raman microscope (inVia^{TM}, Renishaw plc., Gloucestershire, England, UK), as described previously (30, 31). In brief, the tibiae were cleared of soft tissue, and stored in 70% ethanol until testing. The periosteum was stripped off from each sample at the midshaft area using a scalpel and a periosteal elevator. For Raman measurement, tibiae were mounted on a microscope slide using polymer clay with the proximal metaphyseal surface leveled horizontally. About 30 mW of 785 nm laser light was focused onto the cortical surface of the tibiae through a Leica N PLAN L50X/0.50 objective. The scattered Raman signals were collected via the same objective and coupled to a spectrometer inside the inVia^{TM} Raman system. Three spectra per tibia were collected from the midshaft. Each measurement consists of three accumulations of 10 s exposure and has a spectral resolution of ~4 cm^{-1}. All spectra were baseline corrected using a 5th-order polynomial fitting algorithm as previously described using custom written Matlab scripts (32). The peak heights were calculated from Raman signatures of bone, including phosphate $\nu1$ (960 cm^{-1}), phosphate $\nu2$ (431 cm^{-1}), proline (856 cm^{-1}), carbonate (1072 cm^{-1}), amide I (1665 cm^{-1}), and amide III (1245 cm^{-1}). Raman bands from proline and amides (I and III) respectively represent the contribution from collagen and the organic matrix (including collagen and non-collagenous proteins). Spectral parameters for composition analysis were determined as following-collagen mineralization as indicated by mineral-to-collagen ratio (phosphate $\nu1$/proline) (32, 33) and mineral-to-matrix ratio (phosphate $\nu2$/amide III) (34, 35); mineral crystallinity: reciprocal of the full width at half maximum of phosphate $\nu1$ (100x) (33); carbonate-to-collagen ratio: carbonate/proline (31); relative collagen content indicated by collagen-to-matrix ratio (proline/amide I or III) (32).

Quantitative Backscattered Electron Imaging (qBEI)

Bone Mineralization Density Distribution (BMDD) was determined in mutant mice with a conditional allele of *Fkbp10* with and without the *Col1a1* Cre. Bone samples were fixed in 70% ethanol, dehydrated in a graded series of alcohol and embedded in methylmethacrylate. Sectioned bone surfaces of sample blocks were sequentially ground with sand paper followed by polishing with diamond grains (size down to 1 μm) on hard polishing clothes by a precision polishing device (PM5 Logitech, Glasgow, Scotland). Finally, the sample surface was carbon coated by vacuum evaporation (Agar SEM Carbon Coater, Stansted, UK). Quantitative Backscattered Electron Imaging (qBEI) was performed separately in the metaphyseal spongiosa, the epiphyseal spongiosa, and the midshaft cortical bone, as described before (36–39). In total, 14 femurs were analyzed: 7 homozygous floxed without the Cre (3 male samples and 4 female samples) and 7 containing the Cre recombinase (3 male samples and 4 female samples). Note: In one mutant femoral bone the epiphyseal region was missing, therefore BMDD in the epiphyseal region was evaluated only in 6 mutant samples. Bone areas were imaged using a digital electron microscope (DSM 962, Zeiss, Oberkochen, Germany) and gray level histograms were deduced, which were transformed into calcium weight percent (wt% Ca) histograms. The derived BMDD

Author Manuscript Author Manuscript Author Manuscript Author Manuscript

parameters are: (1) CaMean: the mean calcium concentration (weighted mean) (2) CaPeak: the most frequently occurring calcium concentration (the peak position of the BMDD) in the sample, (3) CaWidth: the width of the BMDD distribution (full width at half maximum) reflecting the heterogeneity in matrix mineralization, (4) CaLow: the percentage of low mineralized bone area, which is mineralized below 17.68 wt% Calcium. This cut-off corresponds to the 5^{th} percentile of the reference BMDD in human adults and reflects the portion of bone area undergoing primary mineralization. (5) CaHigh: the percentage of highly mineralized bone matrix, which is mineralized above the 95th percentile value of the corresponding control animals BMDD. This value was defined from the BMDDs of controls at each skeletal site (metaphyseal, epiphyseal, and midshaft cortical bone).

Small Angle X Ray Scattering (SAXS)

For SAXS analyses the same resin embedded blocks were used as for qBEI. 100 μm thin bone sections were obtained by cutting with a low speed diamond saw and subsequent polishing. By this procedure, carbon coating was removed. Bone samples were analyzed with a Nanostar (Bruker AXS, Karlsruhe, Germany) device. The X-ray beam with a wavelength of 1.5418 Å and a diameter of about 200 μm in the focus was generated by an X-ray generator (Bruker AXS, Karlsruhe, Germany) with a rotating copper anode operating at 40kV and 100mA (Cu Kα radiation). The sample-to-detector distance was about 650 mm for the HI-STAR detector (Bruker AXS, Karlsruhe, Germany, pixel size 105.26 μm x 105.26 μm). The calculation of the beam center and the exact sample-to-detector distance was done using a silver behante standard.

The T parameter is defined as:

$$T=\frac{4\Phi(1-\Phi)}{\sigma}$$

with ξ being the mineral volume fraction and σ the total surface of the mineral particles per total tissue volume. Using the assumption that mineral particles have the shape of platelets and that the volume fraction of mineral particles is in the range of $\xi \approx 0.5$, the T parameter represents directly the average mineral particle thickness (40–43). The SAXS data were analyzed by using the software DPDAK (directly programmable data analysis kit) (39, 44).

The average mineral particle thickness (T) was evaluated on 4 different sites (beam diameter: 500μm) on the midshaft cortical diaphysis of each bone sample.

Collagen Fibril Analysis/ Electron Microscopy

Femurs were collected from 3mo old male mice, both epiphyses were removed, and remaining midshaft cortical bone was spun down to remove bone marrow. Bones were then collected in DMEM tissue culture media. Samples were then decalcified using microwave-mediated EDTA treatment. The ends of the bone were trimmed to ensure no trabecular bone remained, along with any tendon fragments. They were then cut into 4 longitudinal strips, followed by cuts to 1mm lengths. An OMNI 2000 homogenizer was used to shear the bone into smaller fragments, followed by homogenization with a glass homogenizer and Teflon

Author Manuscript Author Manuscript Author Manuscript Author Manuscript

plunger (on ice). 5μl of homogenate with the collagen fibrils in solution was placed onto the surface of a glow-discharged carbon coated 600 mesh grid, incubated 1–2 minutes, then 5μl of 4% phosphotungstic acid was added. The grids were dried and examined on a FEI G200 operated at 120KV. Images were taken at a magnification of 150,000x (when printed to a final width of 8 inches) at random locations of the grid, and showed between 1–12 individual collagen fibrils per image. Femurs of two pairs of one *Fkbp10*$^{fl/fl}$ and *Col1-Cre; Fkbp10*$^{fl/fl}$ littermate mouse each were used, 30–37 images per sample were analyzed. The diameter of the collagen fibrils was measured using Image J (45), resulting in a total amount of fibrils measured between 87 and 158 per mouse femur (n=158 for WT and n=100 for mutant in the first pair, n=87 and n=102 in the second pair).

Statistical analyses

For histomorphometry, mass spectrometry and Raman spectroscopy, student s t-test was performed between the two genotypes for each parameter. The BMDD parameters obtained for three tissue ages and the mineral particle thickness (T) were separately analyzed. For μCT and BMDD, we performed 2-way ANOVA to test for the simultaneous effect of gender and genotype, followed by a pairwise comparison using Tukey's multiple comparison post-tests using GraphPad Prism (version 6.0f) and SigmaPlot. Since the differences among the different BMDD parameters between gender and genotype were marginal, we pooled samples from males and females for a repeated measure analysis of the influence of tissue age using GraphPad Prism (version 6.0f). For all analyses, $p < 0.05$ was considered significantly different.

Results

Generation of a conditional Fkbp10 mouse model

Mice previously derived from the European Conditional Mouse Mutagenesis Program (EUCOMM) -ES cells (*Fkbp10*$^{tm1e/+}$) (24) were bred with mice expressing germline flippase mice under the *Gt(ROSA)26Sor* promoter to delete the region between the flippase recognition target (FRT) sites and to create a conditional line (*Fkbp10*$^{fl/fl}$) (Figure 1A). *Fkbp10*$^{fl/fl}$ mice (herein fl/fl) were then bred to the rat *Col1a1* 2.3kb Cre recombinase line to conditionally remove *Fkbp10* in osteoblasts (*Col1-Cre; Fkbp10*$^{fl/fl}$) (Figure 1A) (46). Western blot analysis of calvarial bone extracts from 3-month old mice revealed that FKBP65 expression is absent in *Col1-Cre; Fkbp10*$^{fl/fl}$ mice (herein fl/fl Cre+) compared with Cre-negative controls (herein fl/fl) (Figure 1B). In general, fl/fl Cre+ mice showed no obvious defects in the overall morphology of the skeleton by X-ray imaging (Figure 1C).

Osteoblast derived Fkbp10 is dispensable for postnatal bone mass and does not affect bone cellular composition

To determine if conditional deletion of *Fkbp10* in osteoblasts affects postnatal bone mass and microarchitecture, femurs and spines from 3-month old mice were collected and analyzed by micro-computed tomography (μCT). In femurs, the distal metaphyseal trabecular bone and the cortical bone at the midshaft of femurs in both male and female mice did not show any differences in bone volume over tissue volume (BV/TV), bone surface over bone volume (BS/BV), trabecular number (Tb.N.), trabecular thickness

Author Manuscript Author Manuscript Author Manuscript Author Manuscript

(Tb.Th.), trabecular separation (Tb.Sp.) or cortical thickness (Ct.Th.) in mutant mice when compared with Cre-negative littermate controls (Figure 2A, Supplementary Figure 1A), although significant differences in these parameters was observed between male and female mice, regardless of the genotype (Table S1). Similarly, spines from male mice did not show differences in BV/TV or BS/BV compared with spines of control mice, whereas mild reductions were observed in Tb.N and connectivity density (Conn.D.), which was accompanied by a concomitant increase in Tb.Sp (Figure 2B). Spines from female mice showed no significant changes in these μCT parameters (Supplementary Figure 1B).

We next assessed both static and dynamic histomorphometric parameters from spines of 3-month old male mice to identify changes in osteoblast (bone forming cells) and osteoclast (bone resorbing cells) numbers and osteoblast activity in fl/fl Cre+ mice. Consistent with findings from μCT analyses, only a mild yet significant reduction in Tb.N and increase in Tb.Sp were identified in fl/fl Cre+ mice compared to littermate controls (Figure 3). However, osteoblast numbers (N.Ob/BS), osteoclast numbers (N.Oc/BS) and osteocyte density (N.Ot/B.Ar) were not significantly changed in bone of fl/fl Cre+ mice compared with fl/fl bone. In addition, neither mineral apposition rate (MAR) nor bone formation rate (BFR/BS) were altered in fl/fl Cre+ mice, indicating normal osteoblast function. Furthermore, we did not find any evidence of changes in osteoid (unmineralized bone) parameters (osteoid volume (OV), osteoid surface (OS)) (Figure 3). Taken together, these results indicate that osteoblast derived *Fkbp10* is mostly dispensable for postnatal bone mass and bone cellular composition. Unlike in OI caused by collagen glycine substitutions and/or defects in 3-prolyl-hydroxylation, we do not observe a high bone turnover state at the cellular level.

Osteoblast specific deletion of Fkbp10 leads to impaired bone mechanical properties, altered collagen crosslinking and collagen fibril diameter, and reduced collagen mineralization and crystal size

Next, we examined whether loss of *Fkbp10* in osteoblasts affected bone mechanical properties and mineralization parameters. Three-point bending analysis was performed on femurs obtained from male mice at 3-months of age (n=6 or 8 per group). Although the extrinsic biomechanical parameters (=whole bone level) of femurs of fl/fl Cre+ mice were not different compared with fl/fl femurs, there was a significant decrease in the intrinsic parameters (= tissue level, corrected for femur geometry) of ultimate strength and elastic modulus, suggesting impaired bone tissue properties of bones of the mutant mice. However, unlike in other forms of OI (47, 48), the femurs did not exhibit significantly increased brittleness (determined by reduced plastic displacement and strain) (Table 1).

The quality of collagen cross-linking was assessed in femoral and tibial bone by mass spectrometry to determine telopeptide lysine hydroxylation and HPLC for pyridinoline content. The C-telopeptide domain of type I collagen was underhydroxylated in fl/fl Cre+ bone (Figure 4A and 4C). Consistent with this observation, the total content of mature crosslinks (HP+LP) in fl/fl Cre+ bone was significantly reduced whereas the hydroxylysylpyridinoline/lysylpyridinoline (HP/LP) ratio was unaltered compared with control fl/fl littermate bone (Figure 4D and 4E).

Author Manuscript Author Manuscript Author Manuscript Author Manuscript

In order to examine the effects of *Fkpb10* deletion on collagen fibril diameter, we performed electron microscopy of collagen fibrils in bone samples of fl/fl Cre+ compared with control mice. Quantifying the diameter of collagen fibrils isolated from decalcified cortical bone samples, we observed a subtle trend towards an increased number of fibrils with larger diameters in the mutant samples compared to controls (Figure 5).

To understand if these changes in crosslinking translate into an altered bone material composition, Raman spectroscopy was performed on tibiae bones of male mice. No significant changes were detected in mineral crystallinity or relative collagen content between genotypes (Figure 6). The collagen mineralization (phosphate V1/proline and phosphate V2/amide III), and carbonate-to-collagen ratio reduced in the mutant bone samples, indicating decreased hydroxyapatite and carbonate content with *Fkbp10* mutation.

Additionally, to determine alterations of the mineral content across the femur in fl/fl Cre+ mice, we performed quantitative backscattered electron imaging (qBEI) to assess Bone Mineralization Density Distribution (BMDD) in femurs of male and female mice. Three regions of interest corresponding to different tissue ages were evaluated: the metaphyseal spongiosa, the epiphysis and the midshaft cortical bone (Figure 7A). In both control and mutant mice, the BMDD curve was shifted towards higher mineral content in cortical midshaft bone compared to metaphyseal cancellous bone, reflecting differences in tissue age (Figure 7B). 2-Way ANOVA revealed no interaction between gender and genotype (Table S1). The average mineral content (CaMean) of the bone tissue at the three regions of interest was similar independently of gender or genotype. Only in the metaphyseal spongiosa we found that the heterogeneity in mineralization (CaWidth) and the portion of lowly mineralized bone (CaLow) were affected by gender. At all other sites no major differences were observed (Table S1). Since the differences in BMDD parameters between gender and genotype were marginal, we pooled the samples from males and females for a repeated measures analysis of the influence of tissue age. There was a significant increase in CaMean, CaPeak from the metaphyseal spongiosa, to the epiphyseal spongiosa to the cortical midshaft bone whereas CaLow was decreasing with tissue age (Figure 7C). The same femurs were then subjected to analysis by small angle x-ray scattering (SAXS) to determine mineral particle thickness in cortical midshaft bone. The main effects of gender and genotype cannot be properly interpreted since the interaction term was significant as revealed by 2-Way ANOVA (see Table S1, last row). Post-hoc tests showed that mineral particle thickness was significantly elevated in femurs of male control mice compared to female controls, male and female mutants (Figure 7D).

Discussion

FKBP10 mutations can cause Osteogenesis Imperfecta (OI) and Bruck Syndrome in human patients (11, 13, 22). Given these skeletal phenotypes, as well as the embryonic and postnatal expression patterns of *Fkbp10* in skeletal tissue (24), in this study we characterized the effects of osteoblast specific ablation of *Fkbp10* on the bone phenotype in mice. Unexpectedly, bone mass and most microarchitectural parameters assessed by μCT were not affected by conditional *Fkbp10* deletion, except in vertebrae of male mutant mice, where the Tb.N was decreased and Tb.Sp was increased. Histomorphometric analyses of vertebrae

Author Manuscript Author Manuscript Author Manuscript Author Manuscript

were consistent with trabecular μCT parameters, but did not reveal changes in the osteoid (unmineralized bone matrix) content, osteoblast numbers, osteoclast numbers or osteocyte density, mineral apposition rate or bone formation rate. Thus, deletion of *Fkbp10* in osteoblasts had only minor effects on the quantity or dynamics of bone formation, or balance of osteoblasts and osteoclasts, which are commonly affected in human patients and mouse models of OI (10, 12, 49–52).

Despite the lack of dramatic changes in bone quantity, we observed impaired bone quality parameters in the mutant mice. For instance, biomechanical analysis demonstrated that the femurs of mutant mice were weaker (reduced ultimate strength) and exhibited a decrease in elastic modulus. Unlike other OI models where dramatically increased brittleness was observed, we saw a relatively small, but insignificant, increase in brittleness parameters in these animals. In this study, the reductions in post-yield properties ranged from 12–18% and our sample size was not large enough to be able to detect reductions less than 30% with sufficient power. Based on previous studies showing diminished stable collagen-crosslinking in bone of patients with OI due to *FKBP10* mutations (23, 53), and our studies showing a lack of telopeptide lysine hydroxylation in early calvarial bone of a systemic *Fkbp10* knockout mouse model (24), we evaluated the enzymatic collagen crosslinks in the conditional knockout model (23, 24). The results showed an approximately 50% decrease in HP +LP pyridinoline crosslinks in the long bones of mutant mice compared with littermate controls. Statistical analysis between the total collagen crosslinks and telopeptide lysine hydroxylation showed a strong Pearson correlation with high significance ($r=0.890$, $p=0.007$), indicating that decreased crosslinking in mutant mice is associated with underhydroxylation of telopeptide lysines.

While the ratio of HP/LP was unchanged in mutant mice, the HP + LP amount was decreased, suggesting that telopeptide lysines are underhydroxylated. However, the degree of underhydroxylation of telopeptide lysines in the mutant mice was not as severe as that observed in Bruck syndrome patient bone samples (23). Potential causes for this discrepancy may include contributions of collagen or FKBP65 from additional tissue types. The latter can be partly explained by the presence of residual FKBP65 protein in long bones (Figure S2), which is not observed in calvaria (Figure 1). Alternatively, it could reflect redundancy of another unknown protein in mice that is not as relevant in the human context, which may compensate for the decrease in lysyl hydroxylase activity in mice. In addition, we cannot exclude the possibility that this may be caused by differences in age and the lack of extensive studies from human patient samples. These possibilities will require further investigation to identify the precise molecular mechanisms. Due to the reduction in collagen crosslinks and potential for altered collagen structure, we analyzed the collagen fibril diameters by EM imaging, and found trends to increased collagen fibril diameters in bones of mutant compared with fl/fl mice. However, further studies are needed to correlate the reduction in permanent collagen crosslinking with the increasing trend in fibril diameter.

To determine the effects of osteoblast specific *Fkbp10* deficiency and reduced telopeptide collagen crosslinks on bone material composition in *Fkbp10* conditional mutant mice, we performed Raman spectroscopic analysis. Interestingly, we discovered that conditional deletion of *Fkbp10* in osteoblasts reduced the mineral-to-collagen ratio and the carbonate-to-

Author Manuscript Author Manuscript Author Manuscript Author Manuscript

collagen ratios. While no significant difference was observed in collagen content in relation to the organic matrix, the reduced mineral-to-collagen ratio indicates less mineralization in the *Fkbp10* mutant mice. These results are consistent with Raman spectroscopy analysis performed in fibroblasts of patients with *FKPB10* mutations (53). Further analysis of the bone mineralization density distribution by qBEI revealed no changes in the mean degree of mineralization, heterogeneity of mineralization, or proportions of lowly or highly mineralized bone areas in femurs of mutant mice, although some gender-specific mineralization patterns were observed in the youngest bone tissue (i.e. in the metaphyseal spongiosa) for heterogeneity of mineralization. Together, this indicates that *Fkbp10* is necessary for normal bone mineralization and carbonate/matrix ratios, independently of mineral concentration. Still, these experiments are not sufficient to address the spatial arrangement and size of mineral nanocrystals, which are important contributors to bone quality and biomechanical strength (2, 7, 41). Therefore, we performed SAXS to determine hydroxyapatite crystal size. Interestingly, *Fkbp10* mutant bones exhibited a significant reduction in mineral particle thickness compared to male controls, whereby an interaction between gender and genotype effects cannot be excluded. Taken together, our findings show that although there is no evidence of an overall altered mineral content in *Fkbp10* mutant mice, the ratios of mineral to matrix components are perturbed *in lieu* of the aberrant collagen crosslinking and may provide clues to the role of crosslinking in matrix organization.

The mechanical competence of bone is affected by bone molecular compositions that are arranged in a hierarchical structure. In this study, we investigated mineral properties at multiple scales to determine the potential effects of *Fkbp10* on bone mineralization: qBEI and μCT are surrogates of bone mineral density and distribution at tissue level, Raman spectroscopy assesses mineral-to-collagen ratio microscopically in micron scale, and SAXS analyzes the nanocrystal size of mineral. While no significant differences have been observed in tissue-level mineralization, the amount and crystal size of hydroxyapatite demonstrated notable reduction with *Fkbp10* mutations at micron- and nano-scales respectively although the observed interaction between gender and genotype could interfere with this difference. This finding indicated that *Fkbp10* might affect matrix mineralization at the microscopic level.

In summary, loss of *Fkbp10* in osteoblasts does not result in dramatic changes in bone quantity, but leads predominantly to qualitative changes of the bone material, together with a decrease in permanent collagen crosslinking bonds at telopeptide sites, a decrease in mineral particle thickness, and reduced overall bone biomechanical strength. The phenotype ascertained in this model is clearly less severe than in OI/Bruck Syndrome human patients with loss of function *FKBP10* mutations, possibly due to the lesser reduction of collagen crosslinks. Regardless, the results of this study highlight the importance of molecular changes in collagen crosslinking, bone mineralization, and crystal size on determining bone strength and quality. Further investigation is warranted to develop methods that can enhance bone quality for which this mouse model may provide a valuable tool.

Author Manuscript Author Manuscript Author Manuscript Author Manuscript

Supplementary Material

Refer to Web version on PubMed Central for supplementary material.

Acknowledgments

We would like to thank Megan Bagos for her contribution to micro-CT analysis, and Mahim Jain for his statistical advice and analysis. We would also like to thank Terry Bertin for his critical review of the manuscript text. The authors thank Daniela Gabriel, Petra Keplinger, Sonja Lueger and Phaedra Messmer for careful sample preparations and qBEI measurements.

This work was supported by the NIH P01 HD070394 (BL, DK, DE), F31DE022483 (CL), AR037318 (DE) [www.nih.gov], a research grant from the German Research Foundation/Deutsche Forschungsgemeinschaft (I.G.) [http://www.dfg.de/en/], a Michael Geisman Fellowship from the Osteogenesis Imperfecta Foundation (I.G.) [www.oif.org], the BCM Intellectual and Developmental Disabilities Research Center (HD024064) from the Eunice Kennedy Shriver National Institute Of Child Health & Human Development [https://www.nichd.nih.gov/Pages/index.aspx], the BCM Advanced Technology Cores with funding from the NIH (AI036211, CA125123, and RR024574) [www.nih.gov], the Rolanette and Berdon Lawrence Bone Disease Program of Texas [https://www.mdanderson.org/education-and-research/departments-programs-and-labs/programs-centers-institutes/bone-disease-program-of-texas/index.html], and the BCM Center for Skeletal Medicine and Biology [https://www.bcm.edu/research/centers/skeletal-medicine-biology-bone-disease/cores]. The funders had no role in study design, data collection and analysis, decision to publish, or preparation of the manuscript

Abbreviations

OI	Osteogenesis imperfecta
ER	Endoplasmic reticulum
MEFs	Mouse embryonic fibroblasts
PPIase	Peptidyl-prolyl cis/trans isomerase

References

1. Saito M, Marumo K. Effects of Collagen Crosslinking on Bone Material Properties in Health and Disease. Calcif Tissue Int. 2015 Sep; 97(3):242–61. [PubMed: 25791570]
2. Eyre DR, Weis MA. Bone collagen: new clues to its mineralization mechanism from recessive osteogenesis imperfecta. Calcif Tissue Int. 2013 Oct; 93(4):338–47. [PubMed: 23508630]
3. McNerny EM, Gong B, Morris MD, Kohn DH. Bone fracture toughness and strength correlate with collagen cross-link maturity in a dose-controlled lathyrism mouse model. J Bone Miner Res. 2015 Mar; 30(3):455–64. [PubMed: 25213475]
4. Oxlund H, Barckman M, Ortoft G, Andreassen TT. Reduced concentrations of collagen cross-links are associated with reduced strength of bone. Bone. 1995 Oct; 17(4 Suppl):365S–71S. [PubMed: 8579939]
5. Opsahl W, Zeronian H, Ellison M, Lewis D, Rucker RB, Riggins RS. Role of copper in collagen cross-linking and its influence on selected mechanical properties of chick bone and tendon. J Nutr. 1982 Apr; 112(4):708–16. [PubMed: 6121843]
6. Saito M, Marumo K. Collagen cross-links as a determinant of bone quality: a possible explanation for bone fragility in aging, osteoporosis, and diabetes mellitus. Osteoporos Int. 2010 Feb; 21(2):195–214. [PubMed: 19760059]
7. Bala Y, Farlay D, Boivin G. Bone mineralization: from tissue to crystal in normal and pathological contexts. Osteoporos Int. 2013 Aug; 24(8):2153–66. [PubMed: 23229470]
8. Viguet-Carrin S, Garnero P, Delmas PD. The role of collagen in bone strength. Osteoporos Int. 2006; 17(3):319–36. [PubMed: 16341622]

Author Manuscript Author Manuscript Author Manuscript Author Manuscript

9. Rauch F, Glorieux FH. Osteogenesis imperfecta. Lancet. 2004 Apr 24; 363(9418):1377–85. [PubMed: 15110498]
10. Baldridge D, Schwarze U, Morello R, Lennington J, Bertin TK, Pace JM, et al. CRTAP and LEPRE1 mutations in recessive osteogenesis imperfecta. Hum Mutat. 2008 Dec; 29(12):1435–42. [PubMed: 18566967]
11. Kelley BP, Malfait F, Bonafe L, Baldridge D, Homan E, Symoens S, et al. Mutations in FKBP10 cause recessive osteogenesis imperfecta and Bruck syndrome. J Bone Miner Res. 2011 Mar; 26(3): 666–72. [PubMed: 20839288]
12. Morello R, Bertin TK, Chen Y, Hicks J, Tonachini L, Monticone M, et al. CRTAP is required for prolyl 3-hydroxylation and mutations cause recessive osteogenesis imperfecta. Cell. 2006 Oct 20; 127(2):291–304. [PubMed: 17055431]
13. Alanay Y, Avaygan H, Camacho N, Utine GE, Boduroglu K, Aktas D, et al. Mutations in the gene encoding the RER protein FKBP65 cause autosomal-recessive osteogenesis imperfecta. Am J Hum Genet. 2010 Apr 9; 86(4):551–9. [PubMed: 20362275]
14. Marini JC, Cabral WA, Barnes AM. Null mutations in LEPRE1 and CRTAP cause severe recessive osteogenesis imperfecta. Cell Tissue Res. 2010 Jan; 339(1):59–70. [PubMed: 19862557]
15. Marini JC, Reich A, Smith SM. Osteogenesis imperfecta due to mutations in non-collagenous genes: lessons in the biology of bone formation. Curr Opin Pediatr. 2014 Aug; 26(4):500–7. [PubMed: 25007323]
16. Miao M, Reichheld SE, Muiznieks LD, Huang Y, Keeley FW. Elastin binding protein and FKBP65 modulate in vitro self-assembly of human tropoelastin. Biochemistry. 2013 Nov 5; 52(44):7731–41. [PubMed: 24106871]
17. Cheung KL, Bates M, Ananthanarayanan VS. Effect of FKBP65, a putative elastin chaperone, on the coacervation of tropoelastin in vitro. Biochem Cell Biol. 2010 Dec; 88(6):917–25. [PubMed: 21102654]
18. Ishikawa Y, Vranka J, Wirz J, Nagata K, Bachinger HP. The rough endoplasmic reticulum-resident FK506-binding protein FKBP65 is a molecular chaperone that interacts with collagens. J Biol Chem. 2008 Nov 14; 283(46):31584–90. [PubMed: 18786928]
19. Patterson CE, Schaub T, Coleman EJ, Davis EC. Developmental regulation of FKBP65. An ER-localized extracellular matrix binding-protein. Mol Biol Cell. 2000 Nov; 11(11):3925–35. [PubMed: 11071917]
20. Davis EC, Broekelmann TJ, Ozawa Y, Mecham RP. Identification of tropoelastin as a ligand for the 65-kD FK506-binding protein, FKBP65, in the secretory pathway. J Cell Biol. 1998 Jan 26; 140(2):295–303. [PubMed: 9442105]
21. Duran I, Nevarez L, Sarukhanov A, Wu S, Lee K, Krejci P, et al. HSP47 and FKBP65 cooperate in the synthesis of type I procollagen. Hum Mol Genet. 2015 Apr 1; 24(7):1918–28. [PubMed: 25510505]
22. Barnes AM, Duncan G, Weis M, Paton W, Cabral WA, Mertz EL, et al. Kuskokwim syndrome, a recessive congenital contracture disorder, extends the phenotype of FKBP10 mutations. Hum Mutat. 2013 Sep; 34(9):1279–88. [PubMed: 23712425]
23. Schwarze U, Cundy T, Pyott SM, Christiansen HE, Hegde MR, Bank RA, et al. Mutations in FKBP10, which result in Bruck syndrome and recessive forms of osteogenesis imperfecta, inhibit the hydroxylation of telopeptide lysines in bone collagen. Hum Mol Genet. 2013 Jan 1; 22(1):1–17. [PubMed: 22949511]
24. Lietman CD, Rajagopal A, Homan EP, Munivez E, Jiang MM, Bertin TK, et al. Connective tissue alterations in Fkbp10−/− mice. Hum Mol Genet. 2014 Sep 15; 23(18):4822–31. [PubMed: 24777781]
25. Friedel RH, Seisenberger C, Kaloff C, Wurst W. EUCOMM--the European conditional mouse mutagenesis program. Brief Funct Genomic Proteomic. 2007 Sep; 6(3):180–5. [PubMed: 17967808]
26. Bouxsein ML, Boyd SK, Christiansen BA, Guldberg RE, Jepsen KJ, Muller R. Guidelines for assessment of bone microstructure in rodents using micro-computed tomography. J Bone Miner Res. 2010 Jul; 25(7):1468–86. [PubMed: 20533309]

Author Manuscript Author Manuscript Author Manuscript Author Manuscript

27. Dempster DW, Compston JE, Drezner MK, Glorieux FH, Kanis JA, Malluche H, et al. Standardized nomenclature, symbols, and units for bone histomorphometry: a 2012 update of the report of the ASBMR Histomorphometry Nomenclature Committee. J Bone Miner Res. 2013 Jan; 28(1):2–17. [PubMed: 23197339]
28. Eyre D. Collagen cross-linking amino acids. Methods Enzymol. 1987; 144:115–39. Epub 1987/01/01. eng. [PubMed: 3626870]
29. Hanna SL, Sherman NE, Kinter MT, Goldberg JB. Comparison of proteins expressed by Pseudomonas aeruginosa strains representing initial and chronic isolates from a cystic fibrosis patient: an analysis by 2-D gel electrophoresis and capillary column liquid chromatography-tandem mass spectrometry. Microbiology. 2000 Oct; 146(Pt 10):2495–508. Epub 2000/10/06. eng. [PubMed: 11021925]
30. Bi X, Patil CA, Lynch CC, Pharr GM, Mahadevan-Jansen A, Nyman JS. Raman and mechanical properties correlate at whole bone- and tissue-levels in a genetic mouse model. J Biomech. 2011 Jan 11; 44(2):297–303. Epub 2010/11/03. eng. [PubMed: 21035119]
31. Bi X, Sterling JA, Merkel AR, Perrien DS, Nyman JS, Mahadevan-Jansen A. Prostate cancer metastases alter bone mineral and matrix composition independent of effects on bone architecture in mice--a quantitative study using microCT and Raman spectroscopy. Bone. 2013 Oct; 56(2):454–60. Epub 2013/07/23. eng. [PubMed: 23867219]
32. Bi X, Grafe I, Ding H, Flores R, Munivez E, Jiang MM, et al. Correlations Between Bone Mechanical Properties and Bone Composition Parameters in Mouse Models of Dominant and Recessive Osteogenesis Imperfecta and the Response to Anti-TGF-beta Treatment. J Bone Miner Res. 2016 Sep 20.
33. Ding H, Nyman JS, Sterling JA, Perrien DS, Mahadevan-Jansen A, Bi X. Development of Raman spectral markers to assess metastatic bone in breast cancer. Journal of biomedical optics. 2014; 19(11):111606. [PubMed: 24933683]
34. Kazanci M, Wagner HD, Manjubala NI, Gupta HS, Paschalis E, Roschger P, et al. Raman imaging of two orthogonal planes within cortical bone. Bone. 2007 Sep; 41(3):456–61. [PubMed: 17602910]
35. Zhang Q, Sun X, Yang J, Ding H, LeBrun D, Ding K, et al. ZIP4 silencing improves bone loss in pancreatic cancer. Oncotarget. 2015 Sep 22; 6(28):26041–51. [PubMed: 26305676]
36. Roschger P, Paschalis EP, Fratzl P, Klaushofer K. Bone mineralization density distribution in health and disease. Bone. 2008 Mar; 42(3):456–66. Epub 2007/12/22. eng. [PubMed: 18096457]
37. Misof BM, Roschger P, Baldini T, Raggio CL, Zraick V, Root L, et al. Differential effects of alendronate treatment on bone from growing osteogenesis imperfecta and wild-type mouse. Bone. 2005 Jan; 36(1):150–8. Epub 2005/01/25. eng. [PubMed: 15664013]
38. Fratzl-Zelman N, Morello R, Lee B, Rauch F, Glorieux FH, Misof BM, et al. CRTAP deficiency leads to abnormally high bone matrix mineralization in a murine model and in children with osteogenesis imperfecta type VII. Bone. 2010 Mar; 46(3):820–6. Epub 2009/11/10. eng. [PubMed: 19895918]
39. Fratzl-Zelman N, Bachinger HP, Vranka JA, Roschger P, Klaushofer K, Rauch F. Bone matrix hypermineralization in prolyl-3 hydroxylase 1 deficient mice. Bone. 2016 Apr.85:15–22. [PubMed: 26808442]
40. Fratzl P, Schreiber S, Klaushofer K. Bone mineralization as studied by small-angle x-ray scattering. Connect Tissue Res. 1996; 34(4):247–54. Epub 1996/01/01. eng. [PubMed: 9084633]
41. Fratzl P, Paris O, Klaushofer K, Landis WJ. Bone mineralization in an osteogenesis imperfecta mouse model studied by small-angle x-ray scattering. J Clin Invest. 1996 Jan 15; 97(2):396–402. Epub 1996/01/15. eng. [PubMed: 8567960]
42. Paris O, Zizak I, Lichtenegger H, Roschger P, Klaushofer K, Fratzl P. Analysis of the hierarchical structure of biological tissues by scanning X-ray scattering using a micro-beam. Cell Mol Biol (Noisy-le-grand). 2000 Jul; 46(5):993–1004. Epub 2000/09/08. eng. [PubMed: 10976879]
43. Pabisch S, Wagermaier W, Zander T, Li C, Fratzl P. Imaging the nanostructure of bone and dentin through small- and wide-angle X-ray scattering. Methods Enzymol. 2013; 532:391–413. [PubMed: 24188777]

Author Manuscript Author Manuscript Author Manuscript Author Manuscript

44. Benecke G, Wagermaier W, Li C, Schwartzkopf M, Flucke G, Hoerth R, et al. A customizable software for fast reduction and analysis of large X-ray scattering data sets: applications of the new package to small-angle X-ray scattering and grazing-incidence small-angle X-ray scattering. J Appl Crystallogr. 2014 Oct 1; 47(Pt 5):1797–803. [PubMed: 25294982]
45. Schneider CA, Rasband WS, Eliceiri KW. NIH Image to ImageJ: 25 years of image analysis. Nature methods. 2012 Jul; 9(7):671–5. [PubMed: 22930834]
46. Liu F, Woitge HW, Braut A, Kronenberg MS, Lichtler AC, Mina M, et al. Expression and activity of osteoblast-targeted Cre recombinase transgenes in murine skeletal tissues. Int J Dev Biol. 2004 Sep; 48(7):645–53. Epub 2004/10/08. eng. [PubMed: 15470637]
47. Grafe I, Alexander S, Yang T, Lietman C, Homan EP, Munivez E, et al. Sclerostin Antibody Treatment Improves the Bone Phenotype of Crtap Mice, a Model of Recessive Osteogenesis Imperfecta. J Bone Miner Res. 2015 Dec 30.
48. Grafe I, Yang T, Alexander S, Homan EP, Lietman C, Jiang MM, et al. Excessive transforming growth factor-beta signaling is a common mechanism in osteogenesis imperfecta. Nat Med. 2014 Jun; 20(6):670–5. [PubMed: 24793237]
49. Homan EP, Lietman C, Grafe I, Lennington J, Morello R, Napierala D, et al. Differential effects of collagen prolyl 3-hydroxylation on skeletal tissues. PLoS Genet. 2014 Jan.10(1):e1004121. [PubMed: 24465224]
50. Homan EP, Rauch F, Grafe I, Lietman C, Doll JA, Dawson B, et al. Mutations in SERPINF1 cause osteogenesis imperfecta type VI. J Bone Miner Res. 2011 Dec; 26(12):2798–803. [PubMed: 21826736]
51. Morello R, Rauch F. Role of cartilage-associated protein in skeletal development. Curr Osteoporos Rep. 2010 Jun; 8(2):77–83. [PubMed: 20425614]
52. Cabral WA, Perdivara I, Weis M, Terajima M, Blissett AR, Chang W, et al. Abnormal type I collagen post-translational modification and crosslinking in a cyclophilin B KO mouse model of recessive osteogenesis imperfecta. PLoS Genet. 2014 Jun.10(6):e1004465. [PubMed: 24968150]
53. Barnes AM, Cabral WA, Weis M, Makareeva E, Mertz EL, Leikin S, et al. Absence of FKBP10 in recessive type XI osteogenesis imperfecta leads to diminished collagen cross-linking and reduced collagen deposition in extracellular matrix. Hum Mutat. 2012 Nov; 33(11):1589–98. [PubMed: 22718341]

Author Manuscript Author Manuscript Author Manuscript Author Manuscript

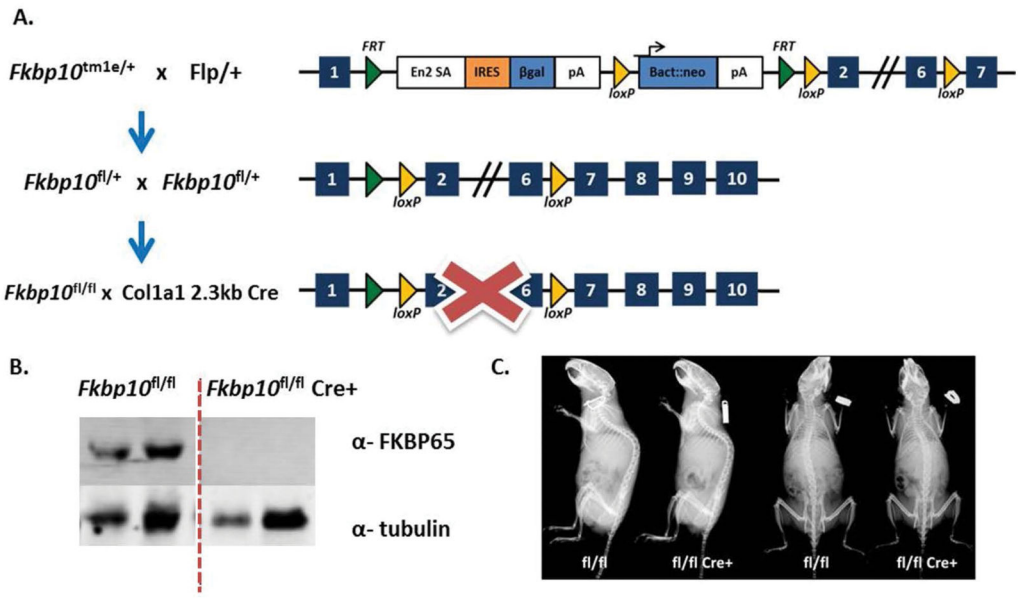

Figure 1. Conditional Knockout of *Fkbp10*

(A) *Fkbp10* EUCOMM mice were bred to transgenic mice expressing germline flippase to generate a conditional allele. The *Col1a1* 2.3kb Cre was used to conditionally ablate *Fkbp10* in osteoblasts. (B) Western blot of FKBP65 deletion in 3-month old calvarial samples. (C) Radiographs of 3-month old male mice do not show any gross phenotypes.

Author Manuscript Author Manuscript Author Manuscript Author Manuscript

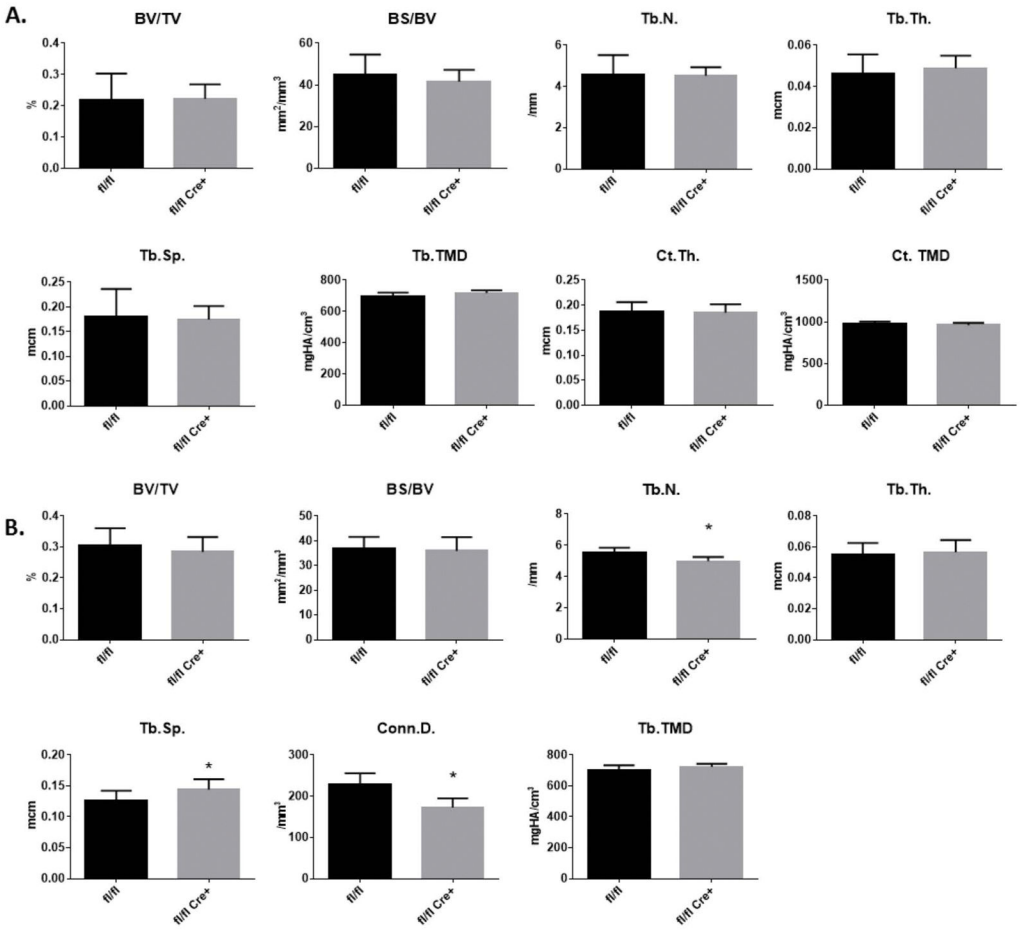

Figure 2. Quantitative µCT Analysis

Bone parameters by µCT of (A) femurs and (B) spines in 3-month old male mice. Parameters as follows: bone volume/tissue volume (BV/TV), bone surface/bone volume (BS/BV), trabecular number (Tb.N), trabecular thickness (Tb.Th.), trabecular separation (Tb.Sp.), connectivity density (Conn.D.) Data are presented as means ± SD. *p<0.05 (Student's t-test), n=9 for control and n=7 for mutant.

Author Manuscript Author Manuscript Author Manuscript Author Manuscript

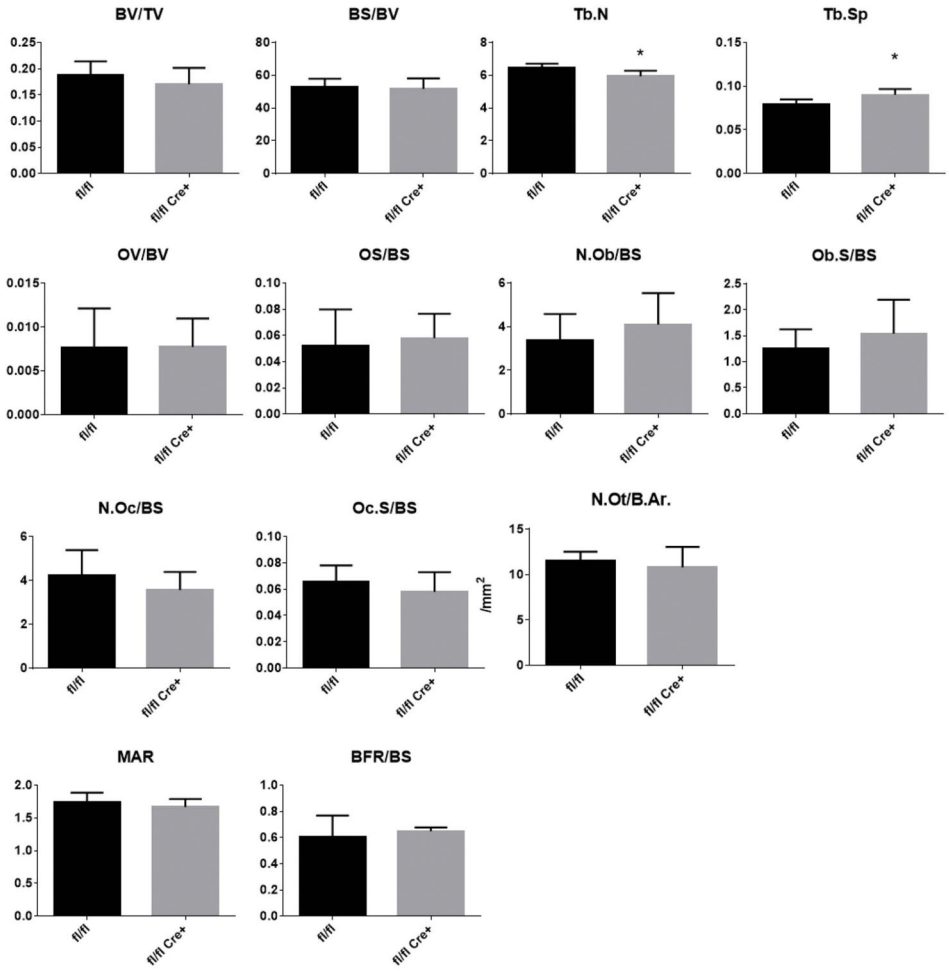

Figure 3. Histomorphometric Analysis

Histomorphometric analysis of the L4 vertebrae of 3-month old male mice. Parameters are bone volume/ tissue volume (BV/TV), bone surface/bone volume (BS/BV), trabecular number (Tb.N), trabecular separation (Tb.Sp.), osteoid volume/bone volume (OV/BV), osteoid surface/bone surface (OS/BS), number of osteoblasts/bone surface (N.Ob/BS), osteoblast surface (Ob.S./BS), number of osteoclasts/bone surface (N.Oc./BS), osteoclast surface/bone surface (Oc.S/BS), number of osteocytes/bone area (N.Ot./B.Ar), mineral apposition rate (MAR) and bone formation rate (BFR/BS). Values are means ± SD, *$p<0.05$ by Student's t-test. N=7 per group.

Author Manuscript Author Manuscript Author Manuscript Author Manuscript

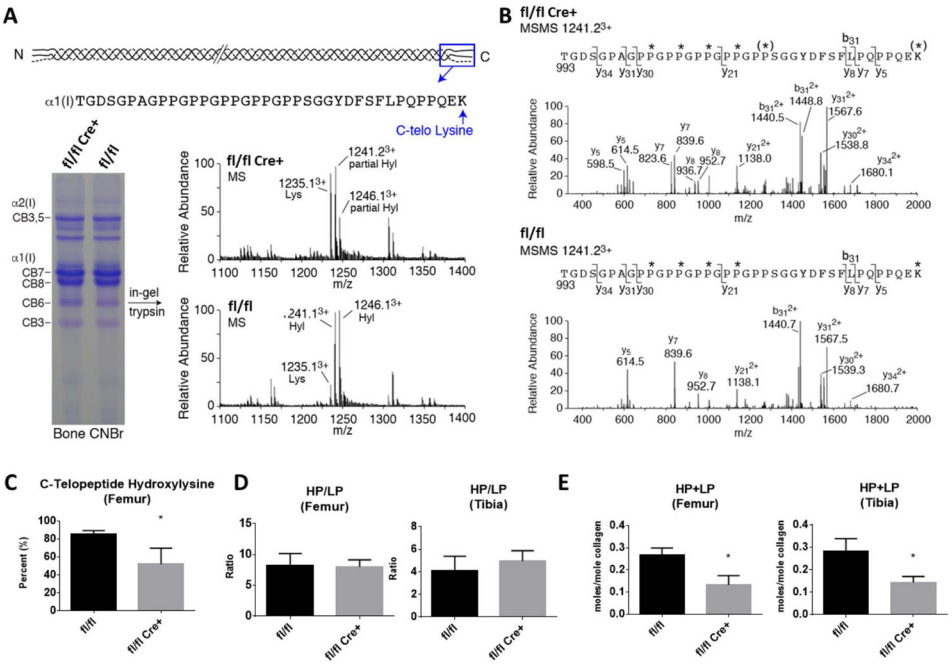

Figure 4. Post-translational Collagen Modification and Cross-linking

(A) SDS-PAGE of CNBr digested bone and mass spectral analysis of in-gel trypsin digested α1(I) CB6. The C-terminal tryptic peptide shown reveals the α1(I) C-telopeptide lysine hydroxylation state. (B) MS/MS fragmentation spectra of parent ion (1241.2^{3+}) from fl/fl and fl/fl Cre+ bone α1(I). The fl/fl Cre+ spectrum shows both lysine and hydroxylysine fragment ions, whereas only hydroxylysine fragment ions are present in the control. (C) Quantitation of bone collagen C-telopeptide lysine hydroxylation by mass spectrometry. (D) The hydroxylysylpyridinoline/lysylpyridinoline (HP/LP) ratio was not altered in mutant compared to control littermate bones, but the total crosslinks (HP+LP) were significantly reduced in both the femur and tibia (E). Statistical analyses were performed by Student's t-test for each parameter. N=3–4 per group, values in mean ± SD, *p<0.05.

Author Manuscript Author Manuscript Author Manuscript Author Manuscript

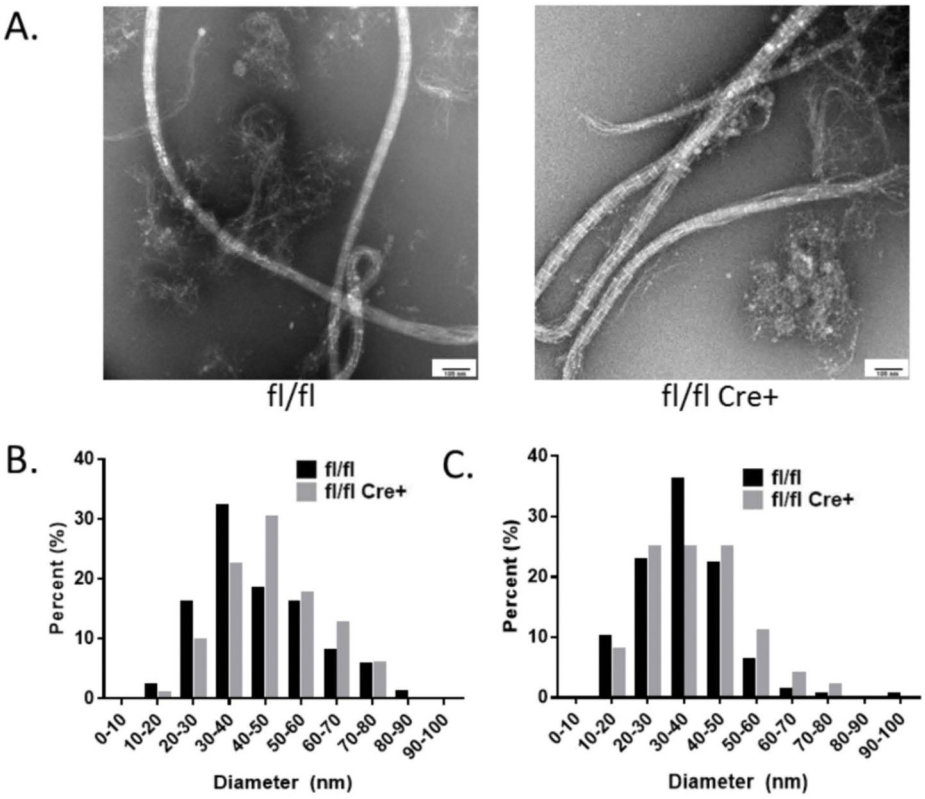

Figure 5. Collagen Fibril Diameter

(A) Representative electron microscopy images of collagen fibrils, extracted from femoral bones of fl/fl Cre+ mice and control littermates, are shown from paired samples. (B and C) Quantification of the diameters of collagen fibrils are shown from two littermate pairs of control and mutant mice. 87–158 individual fibrils were measured in 30–37 separate image fields from each bone.

Author Manuscript Author Manuscript Author Manuscript Author Manuscript

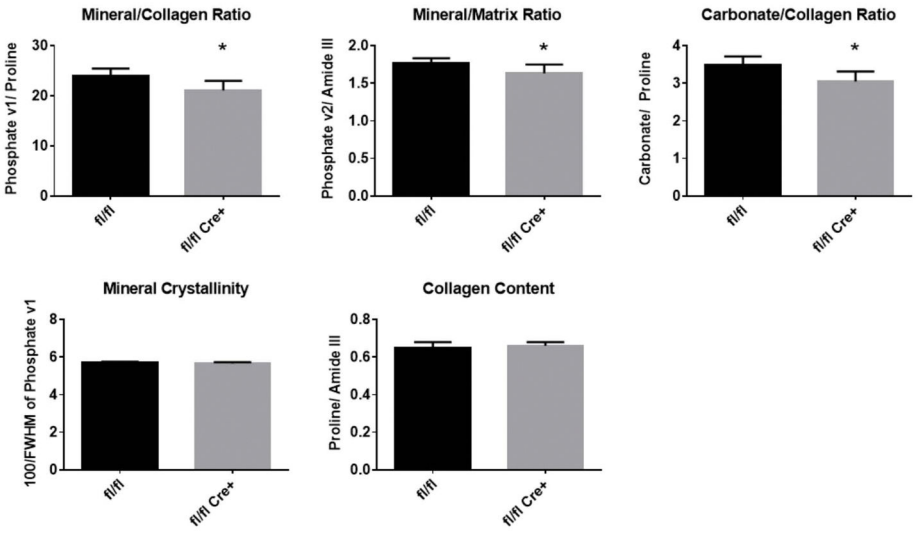

Figure 6. Raman Spectroscopy

Mineralization (phosphate V1/proline and phosphate V2/amide III), and carbonate/matrix (carbonate/proline) ratios were significantly reduced in tibias from 3-month old male mice. Crystallinity (100/phosphate V1 width) and protein/matrix (amide/CH2) were unchanged. n=7, values in mean ± SD, *p<0.05.

Author Manuscript Author Manuscript Author Manuscript Author Manuscript

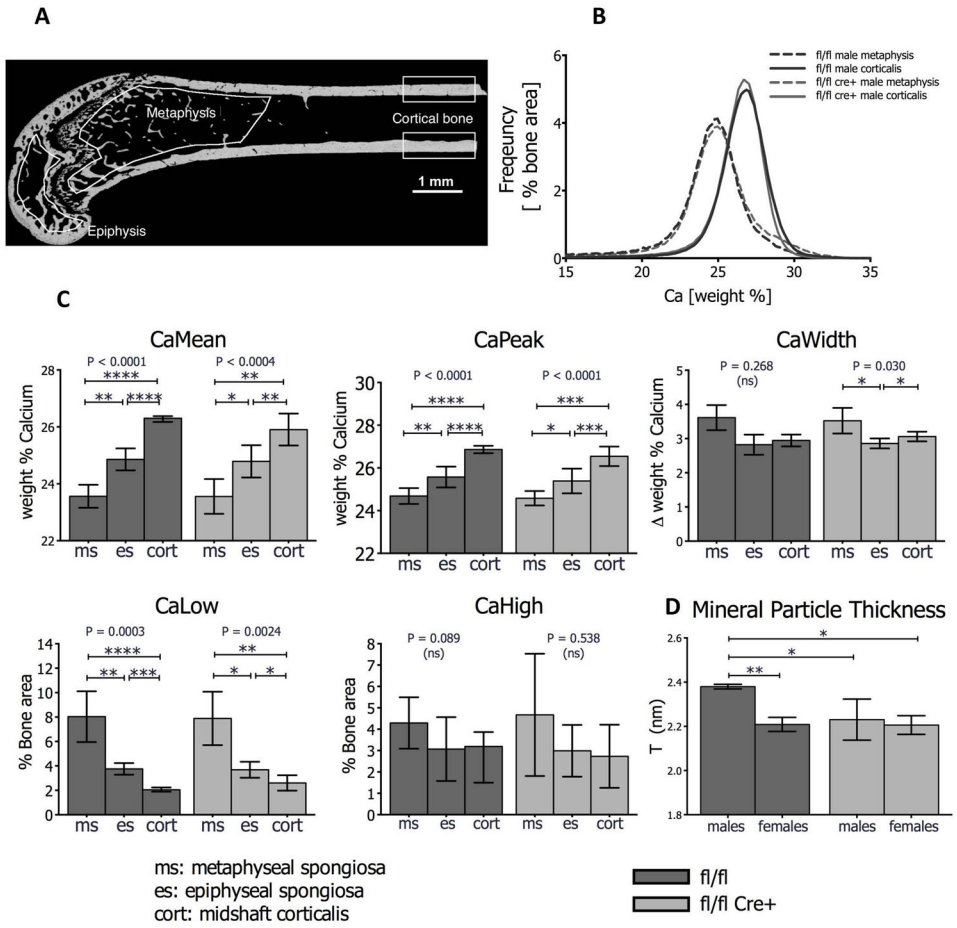

Figure 7. Bone Mineralization Density Distribution (BMDD) of Femurs

(A) Quantitative backscattered electron image (qBEI) of a wild type femur showing three regions of interest with different bone tissue age (metaphysis, epiphysis, cortical bone). (B) Example of BMDD curves in cortical bone and the metaphysis of fl/fl control and fl/fl Cre+ mice. Note that cortical bone is more highly mineralized than metaphyseal cancellous bone, reflecting higher (less remodeled) tissue age. However, at the same skeletal site, BMDD curves are unchanged between groups. (C) Results of Repeated Measures ANOVA with multiple comparisons. CaMean and CaPeak increase significantly in fl/fl controls as well as in fl/fl Cre+ mutants from metaphysis, to epiphysis to cortical bone, whereas CaLow decreases progressively with tissue age. CaWidth and CaHigh are not significantly affected by tissue age. For each point n=7 (three males and four females, pooled). Data are mean (±SD) *p<0.05, **p<0.01, ***p<0.001, ****p <0.0001. (D) Mineral particle thickness (T parameter) determined by small angle x-ray scattering (SAXS) is reduced in mutant male and female femurs compared to male controls, but not in female counterparts. N =3 (males) or 4 (females). Values in mean (± SD). Statistical analyses two-way ANOVA with multiple comparisons. *p<0.05; **p<0.01.

Author Manuscript Author Manuscript Author Manuscript Author Manuscript

J Bone Miner Res. Author manuscript; available in PMC 2018 June 01.

Table 1

Biomechanical testing of femurs

Three-point bending tests were performed on femurs of male mice at 3 months of age. Statistical analyses performed by t-test for each parameter (* $p<0.05$). Parameters with grey background are intrinsic and adjusted according to the geometry of the femurs.

	Group	N	Mean	Std. Deviation	P value
Yield Load (N)	fl/fl	8	12.84	4.01	0.490
	fl/fl Cre+	6	11.44	3.09	
Ultimate Load (N)	fl/fl	8	17.40	3.90	0.630
	fl/fl Cre+	6	16.52	2.11	
Fracture Load (N)	fl/fl	8	12.71	3.11	0.364
	fl/fl Cre+	6	14.09	1.97	
Stiffness (N/mm)	fl/fl	8	117.24	25.50	0.167
	fl/fl Cre+	6	97.40	24.16	
Elastic Energy (N*mm)	fl/fl	8	0.892	0.431	0.773
	fl/fl Cre+	6	0.831	0.302	
Plastic Energy (N*mm)	fl/fl	8	8.38	2.21	0.251
	fl/fl Cre+	6	7.00	1.96	
Elastic Displacement (mm)	fl/fl	8	0.111	0.023	0.531
	fl/fl Cre+	6	0.119	0.026	
Plastic Displacement (mm)	fl/fl	8	0.549	0.060	0.161
	fl/fl Cre+	6	0.471	0.132	
Ultimate Strength (MPa)	fl/fl	8	104.89	7.48	***0.031**
	fl/fl Cre+	6	95.00	7.50	
Elastic Modulus (MPa)	fl/fl	8	3586.28	618.84	***0.021**
	fl/fl Cre+	6	2741.15	538.56	
Resilience (MPa)	fl/fl	8	1.060	0.400	0.625
	fl/fl Cre+	6	0.964	0.302	
Elastic Strain (%)	fl/fl	8	0.022	0.006	0.496
	fl/fl Cre+	6	0.025	0.007	